




# Design and optimization the wear characteristics for Al7178/TiO<sub>2</sub>/B4C/FA central hybrid composite

P. Anusha<sup>1</sup> · M. Naga Swapna Sri<sup>1</sup> · S. Vijayakumar<sup>2</sup> · T. V. Janardhana Rao<sup>3</sup> · Prabhu Paramasivam<sup>4</sup> · S. Jeyakrishnan<sup>5</sup> · Kuldeep Kumar Saxena<sup>6</sup> 

Received: 27 January 2023 / Accepted: 17 April 2023

© The Author(s), under exclusive licence to Springer-Verlag France SAS, part of Springer Nature 2023

## Abstract

In this research process, Al 7178 is considered as base material, boron carbide (B4C), Titanium dioxide and Flyash are utilized as reinforcement elements to improve the wear behavior. The sample of the composite is prepared by Stir casting method. The amount of all reinforcements (3%) is constant. As per the central composite design, wear tests are performed on pin on disc apparatus with alteration of factors level. The chosen factors are load (15 N, 25, 35 N) and sliding speed (3, 6 and 9 m/s) and sliding distance (350, 400, 450 m). The observation experiment results shows that Maximum wear rate is recorded as 0.01582 mm<sup>3</sup>/Nm for a load of 25 N, slide distance of 400 m and slide speed of 6 m/s. The minimum Wear rate is attained as 0.00748 mm<sup>3</sup>/Nm at parameters combinations of 35N, 450 m and 9 m/s. Analysis of variance (ANOVA) showed that load, and the interaction between load and sliding distance have the most significant parameters on wear rate trailed by sliding speed.

**Keywords** AMCs · Optimization · Wear behavior

## 1 Introduction

Al matrix composites are generally recommended for making different light objects in many cases [1]. The characteristics of Al alloy were created by utilizing nano and tiny reinforcements ceramic grains like TiC, SiC. Most of the additions with Al were silicon carbide and alumina for enhancing

mechanical characteristics [2, 3]. Casting is a manufacturing procedure used for this purpose by pouring the heated liquid into a solid object or component liquid substance inside a mold with a desired shape [4]. Porosity is reduced by these cast products and mix the grain particles equally [5]. Al alloy 7xxx series is frequently used in aerospace structures field because of their outstanding properties and light weight. However, the alloys' weak corrosion resistance makes them less significant [6, 22]. The aluminum alloy AA7178 from the different 7xxx family alloys is chosen for this work. Reinforcing particles can improve the qualities of aluminum alloys, such as their strength, modulus, and wear resistance [7, 23]. In these investigations, wear control factors were examined. It is mostly to determine their influence on wear rate depending on load [8, 24] and wear rate which was affected by velocity, reinforcement in and other influences [9, 25]. Using the stir casting process, the 7075 aluminum-zinc alloy is reinforced with mixtures of ZrB<sub>2</sub> particles. At weight percentages of 5, 10, and 15, the reinforcements were incorporated into the base alloy. The hardness and density of the composites were significantly higher than those of the parent alloy. Mechanical characteristics including the UTS and YS showed a considerable variation. Composite weighing 15 wt% showed an improvement in tensile strength

✉ Kuldeep Kumar Saxena  
saxena0081@gmail.com

<sup>1</sup> Department of Mechanical Engineering, P V P Siddhartha Institute of Technology, Vijayawada, India

<sup>2</sup> Department of Mechanical Engineering, BVC Engineering College (Autonomous), Odalarevu, Andhrapradesh 533210, India

<sup>3</sup> Department of Electronics and Communications Engineering, BVC Engineering College (Autonomous), Odalarevu, Andhra Pradesh 533210, India

<sup>4</sup> Department of Mechanical Engineering, Engineering and Technology, Mattu University, Mettu 318, Ethiopia

<sup>5</sup> Department of Mechanical Engineering, ARM College of Engineering and Technology, Maraimalainagar, Chennai 603209, India

<sup>6</sup> Division of Research and Development, Lovely Professional University, Phagwara 144411, India

of roughly 34% as compared to base alloy [10]. ZrB<sub>2</sub> can improve the mechanical and corrosion performances of Al 7178, and AA7178-ZrB<sub>2</sub> metal matrix composite had better corrosion resistance than the parent alloy. The rate of corrosion resistance, hardness, impact strength, and tensile strength was enhanced by gradually increasing the weight % of ZrB<sub>2</sub> particles in the AA7178 matrix. By including 10% ZrB<sub>2</sub> particles into the AA7178 matrix, the hardness was enhanced by approximately 25% and the ultimate tensile strength by 15% [11]. Hybrid Al/Al<sub>2</sub>O<sub>3</sub>/Gr composites have high wear and friction, As the TiC content in the AA7178 composites improved wear rate and coefficient of friction. decreased [12]. The wear resistance of AA7075 composites integrating Si<sub>3</sub>N<sub>4</sub> particles from stir casting is examined, SiC reinforcement decreased the volumetric wear loss of Al7075/SiC matrix [13]. On a pin-on-disc machine, SiC/TiO<sub>2</sub> particulate composites in aluminium alloy LM25 is examined. C.O.F. & wear decreased with increasing TiO<sub>2</sub> content [14]. A resource material for the cement industry and production facilities of building products is fly ash, which is generated by thermal power plants based on coal. Additionally, it is a building material used in the construction of roads and flyover embankments. After stir casting a 6061 Al-Al<sub>2</sub>O<sub>3</sub> metal matrix composite, the mechanical and wear characteristics are assessed. The melt stirring method, which incorporates preheat reinforcement and three phases of mixing, has been utilized to effectively produce composites, including 6061Al with 6 to 12 weight percent Al<sub>2</sub>O<sub>3</sub>. In optical micrographs of stir-cast composites, alumina particles are dispersed rather equally throughout the 6061 Al metal matrix [15]. With AA7075 acting as the matrix material, alumina, boron carbide, and carbon are reinforced. The composites' flexural, tensile, and wear characteristics are also studied [16]. Al/SiC/mica composites that are made using the stir casting technique is being studied for their wear and mechanical characteristics Energy dispersive X-ray (EDX) detector is used to analyze the chemical composition. Al/10SiC-3mica composites provide the best strength and hardness. The wear loss of the composites is improved by an increase in mica's mass fraction [29]. S. Gopalakrishnan analyses the dry sliding wear properties of AMC using POD equipment after Al-TiCp castings with various volume fractions of TiC were created in an argon atmosphere. It is found that the wear resistance of the composite increased with larger% of TiC addition [30]. Liquid forging is supported to create SiCp/2A50 composite materials. SiCp/2A50 of the pit initiation has virtually the same corrosion resistance as the matrix alloy. It is been discovered that once pits begin, the corrosion damage caused by pitting is increased because crevices emerge between the reinforcement and the matrix. The composite and the matrix alloy's resistance to pitting corrosion in chloride-containing environments is significantly reduced

by the SiCp. SiCp speeds up the corrosion rate of composite materials, causing them to corrode at a rate that is higher than that of aluminum alloys [31]. The review of the literature indicated the importance of creating hybrid reinforced 7xxx series composites with high strength and low weight. However, there hasn't been much work done to optimize the wear rate process variables. The innovative aspect of this study is the use of stir casting to create Al7178/TiO<sub>2</sub>/B4C/FA hybrid composites. Additionally, the wear rate of the cast samples was examined, along with the most effective wear parameters and the reinforcement's contribution to the composites' improved wear behavior. We were able to choose the optimal parameters from the selected variables Load (LD), Sliding Speed (SS), and Sliding Distance (SD) using CCD method. Al7178/TiO<sub>2</sub>/B4C/FA composites are used in many industrial products such as Aircraft components, Boilers, Condensers, Heat exchangers and Petroleum refineries.

## 2 Preparation of the samples

First level is to metal Collection in the process then making sample of Al7178 matrix composites via stir-cast process. Following that, produced specimens using ASTM standards were collected to undergo exams for wear analysis [26]. Most often, the casting method is utilized to form items into the required shape using mold components. In this experiment, the main component of the stirrer is constructed of stainless steel, and it is used to mix Al-alloy with certain reinforcements at different speeds. Stirrer rotation is kept between 600 and 800 rpm while furnace inserts controls heat to melt solid metal and particles. Prior to the addition of particles, the furnace crucible and reinforcements (B4C, TiO<sub>2</sub>, and FA) should be preheated to 300 °C. After a solid is transformed into molten metal and transported to specially constructed dies, a stir rod needs electricity to undertake mixing operations with the ingredients. The setup of stir casting is shown in Fig. 1 and also chemical elements and properties of 7178 Al displayed in Tables 1 and 2 respectively.

## 3 Dry sliding wear test

Figure 2 depicts pin on the disc is utilized to examine dry sliding wear behavior of prepared composites according to ASTM G99 Standard [17, 27]. This test is carried out at Wear Check Laboratories India Pvt. Ltd, Chennai. The produced specimen was first cleaned with acetone before being weighted to determine its initial mass with a machine-based digital electronics balance. The sample was held against the steel disc's rotation. The track diameter was maintained throughout each wear study while LD, SS and SD were all varied with the specific range. Until the contact surface wears

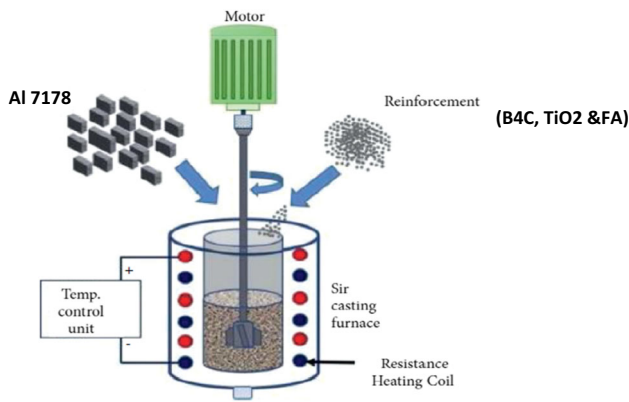


Fig. 1 Stir casting arrangement

down, the load forces the arm to maintain contact specimen with the disc. The friction is produced which leads to material removal on the sample. Utilizing an electronic scale, the weight loss of each specimen was determined following thorough washing with acetone solution [28]. Wear rate is determined based on the weight loss of the sample during the wear tests. The level of all parameters selected illustrated in Table 2.

#### 4 Design of experiment and parameters

The experiments were carried out in accordance with the CCD in RSM design. To determine the relationship between a number of different independent input variables and output reactions, CCD was used for estimating the second-order response surface and for an optimization approach [18–20]. The optimization process has been done with an assistance of design expert software with quadratic model. The design’s variables were divided into three levels (low, medium, and high, which were coded as – 1, 0, and + 1, and a total of 20 runs with three replicates were performed to optimize the level of the selected variables [32, 33].

#### 5 Result and discussion

The experimental results of the wear rate according to CCD design on Al-based composites are shown in Table 3. The three parameters LD, SS, and SD are varied at different levels to evaluate WT. 20 tests are carried out in accordance

Table 2 Wear test factors

Parameters	Level 1	Level 2	Level 3
LD	15	25	35
SD	350	400	450
SS	3	6	9



Fig. 2 Pin on disc equipment

with the CCD with modifications to chosen parameters. The total wear results are exposed in Fig. 3. The maximum and minimum wear rate are recognized as 0.01582 mm<sup>3</sup>/Nm and 0.00748 mm<sup>3</sup>/Nm respectively. The grouping of factor levels for highest WT is at LD2-SD2-SS2 with the values of 25 N, 400 m and 6 m/s and minimum WT is at LD3-SD2-SS3 with values of 35 N, 450 m/s and 9 m/s correspondingly. The results showed that WT is pretty much exactly proportional to the applied Load and distance of the disk which means WT improves more when both factors LD & SD are upraised (Fig. 4).

The ANOVA test focuses on variance-based mean differences to determine if there is a statistically significant distinction among two or more category groups [21, 34, 35]. An ANOVA illustrates the significance of many parameters and how they interact with one another with a 95% confidence range. If P is 0.05 or below, the influence of the parameter is deemed significant. There are no crucial model terms in this situation. Models are not significant if the value exceeds 0.1000. Model reduction may enhance the model’s complexity if it contains a large number of unnecessary terms. Table 4 showed the quadratic model in the ANOVA. The interface

Table 1 Al 7178 chemical elements

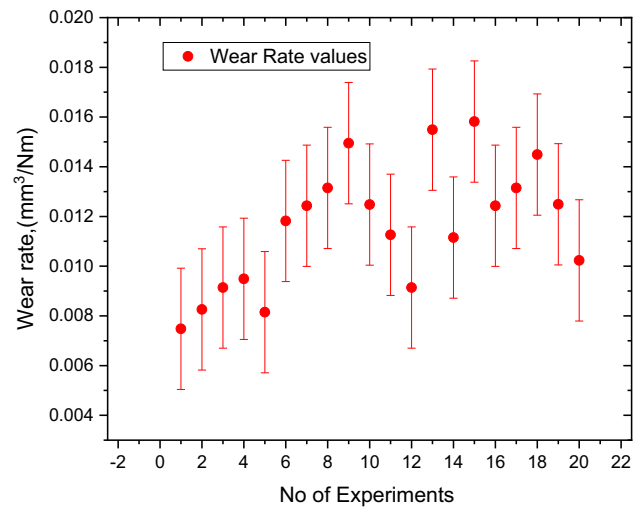
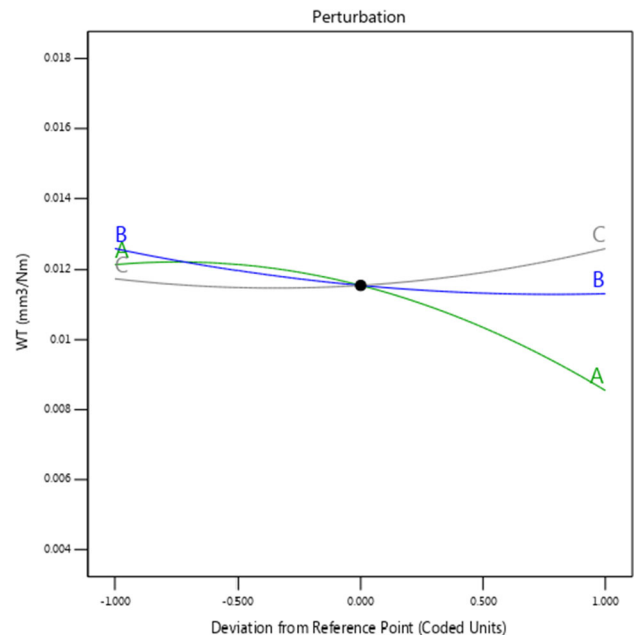
Elements	Cr	Cu	Fe	Mg	Mn	Si	Ti	Zn	Al
%	0.18	0.9	0.5	2.5	0.09	0.23	0.12	6.9	Balance

**Table 3** Factors combination along with Wear result

Std	Run	LD (N)	SD (m)	SS (m/s)	WT ( $\text{mm}^3/\text{Nm}$ )
8	1	35	450	9	0.00748
2	2	35	350	3	0.00826
10	3	35	400	6	0.00914
4	4	35	450	3	0.00949
19	5	25	400	6	0.00815
16	6	25	400	6	0.01182
9	7	15	400	6	0.01243
5	8	15	350	9	0.01315
3	9	15	450	3	0.01495
6	10	35	350	9	0.01248
15	11	25	400	6	0.01126
20	12	25	400	6	0.00914
11	13	25	350	6	0.01549
1	14	15	350	3	0.01115
17	15	25	400	6	0.01582
13	16	25	400	3	0.01243
7	17	15	450	9	0.01315
14	18	25	400	9	0.01449
18	19	25	400	6	0.01249
12	20	25	400	6	0.01023

between LD and SD is revealed in Fig. 5. It is noticed that the WT is increased while increase LD from 15 to 30 N but WT reduction is noticed while increasing SD values from 350 to 450 m. Figure 6 showed the interaction between LD and SS on WT. Wear rate is decreasing by increasing SD and increment of WR value by increasing LD. The more heat is obtained while the sample contact under various circumstances with disc might be too responsible for the change of Wear rate. Similarly, the effect of interaction of wear parameters of other conditions (SS and SD) are reported in the Fig. 6. WR is decreasing by increasing SD and decreasing by increment of SD. From ANOVA results, application of load on sample is first factor to increase wear rate, followed by Sliding distance and sliding speed and the combination parameters of LD\*SD, LD\*SS and SS\*SD (Fig. 7). A predicted against actual plot shows a model effect and compares it to the null model. The actual WT values and the values the model predicts are compared using a scatter plot. The plot shows the actual value fixed in X-axis and the predicted value in Y-axis as shown in Fig. 8. During the observation of Actual with predicted values, the WT is nearly contiguous.

The perturbation graph makes it easier to compare each factor's (LD/SD/SS) impact at a specific location in the design space of WT. Plotting the response involves varying just one element over its range while keeping the other variables constant. Design-Expert automatically places the

**Fig. 3** Wear test overall result**Fig. 4** Perturbation plot

reference point at the middle of all the factors. It is observed that A term is specified as load factor, B is notified as SD and C is SS in the Fig. 4 and the load is more deviated from center point which means wear rate is increased more due to more load whereas SD is acted as moderate factor and finally SS term contribution is very less on wear rate increment. With help of design expert software, wear rate values can be determined approximately. Figure 9 is showing the wear rate as  $0.0115002 \text{ mm}^3/\text{Nm}$  due to allotting values for input factors load of 24.0855 N, sliding diameter of 427.548 m and sliding distance of 6.26674 m/s. In our work, the wear resistance is improved by adding the three different reinforcements at constant weight percentage (3%).

**Table 4** ANOVA outcomes

Source	SS	df	MS	F	p
Model	0.0001	9	8.063E-06	8.73	0.0301
A-LD	0.0000	1	0.0000	6.95	0.0249
B-SD	5.691E-06	1	5.691E-06	1.22	0.0492
C-SS	2.527E-06	1	2.527E-06	0.5436	0.4779
LD*SD	7.163E-06	1	7.163E-06	7.54	0.0242
LD*SS	5.050E-07	1	5.050E-07	0.1086	0.7485
SD*SS	0.0000	1	0.0000	2.71	0.1310
LD <sup>2</sup>	6.961E-06	1	6.961E-06	1.50	0.2491
SD <sup>2</sup>	2.369E-06	1	2.369E-06	0.5096	0.4917
SS <sup>2</sup>	5.471E-06	1	5.471E-06	1.18	0.3034
Residual	0.0000	10	4.648E-06		
Lack of fit	9.904E-06	5	1.981E-06	0.2708	0.9110
Error	0.0000	5	7.316E-06		
Total	0.0001	19			

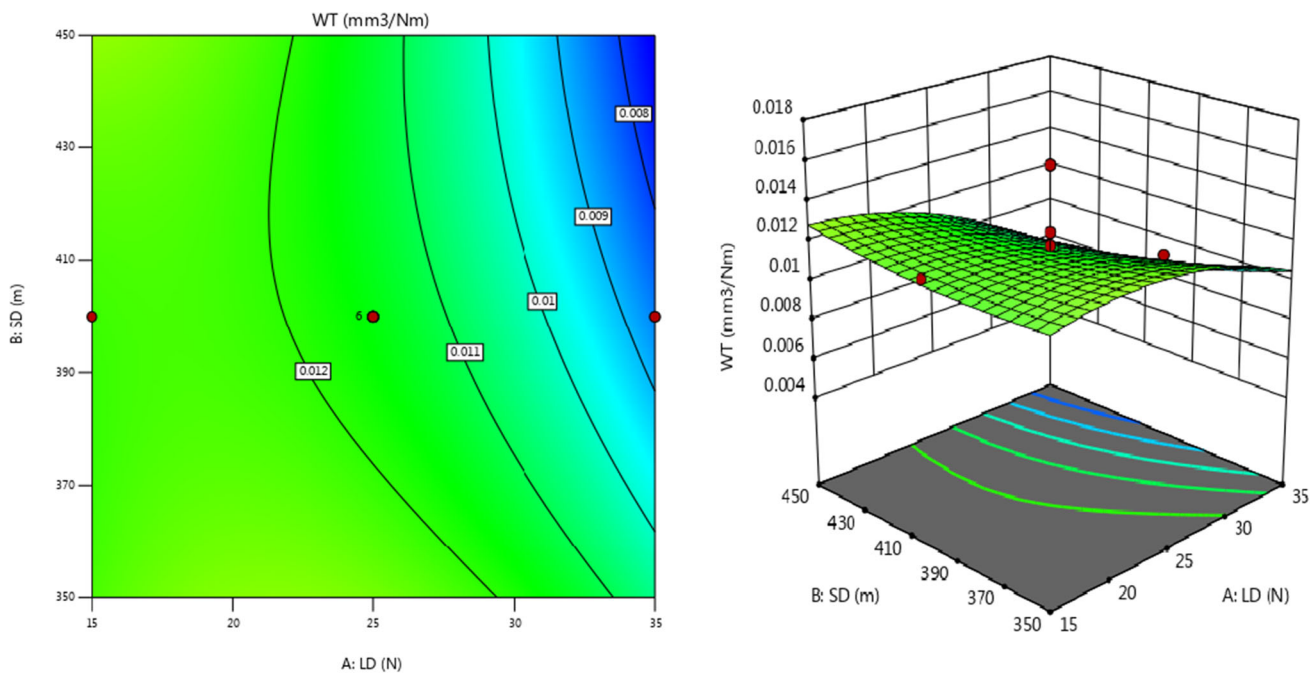


**Fig. 5** LD/SD interaction plot

### 6 Predicted-model equation

Regression analysis or equation is the examination of connection between dependent variable of LD, SS and SD and independent variable of WT as it depicts how dependent variable will change when the independent variable changes due to factors, the predicted value of wear rate is found at modeling process in the optimization software is shown in Eq. (1)

$$\begin{aligned}
 WT = & +0.003689 + 0.001129 LD - 0.000046 SD \\
 & + 0.002450 SS - 1.89250E-06 LD * SD + 8.37500E \\
 & - 06 LD * SS - 8.35833E-06 SD * SS - 0.000012 \\
 & + 1.63238E - 07 SD^2 + 0.000069 SS^2 \quad (1)
 \end{aligned}$$

For a model to be considered trustworthy, it must be able to anticipate the reaction with some degree of accuracy before

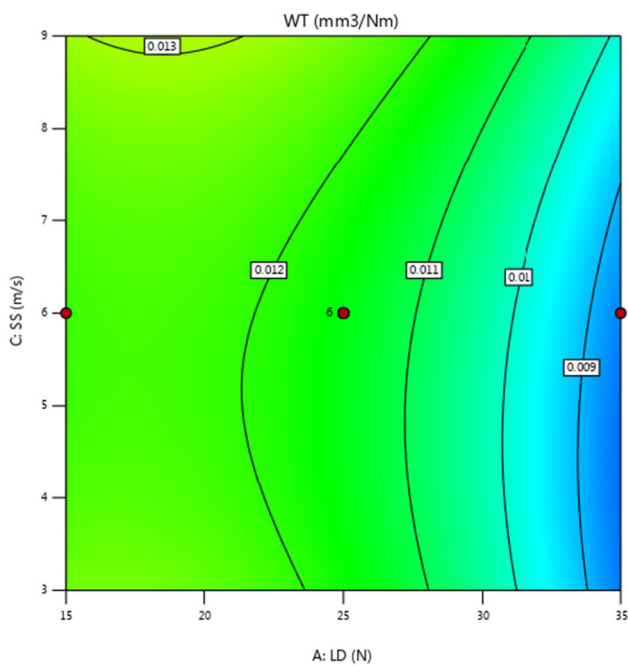


Fig. 6 LD/SS interaction plot

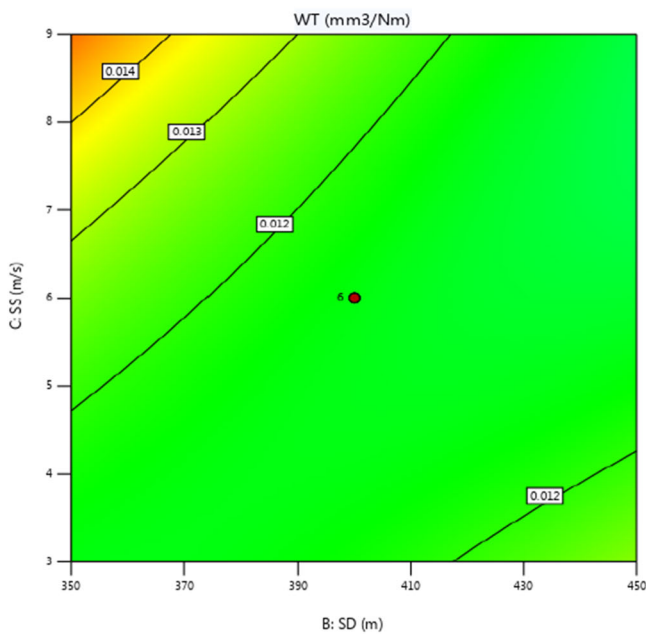
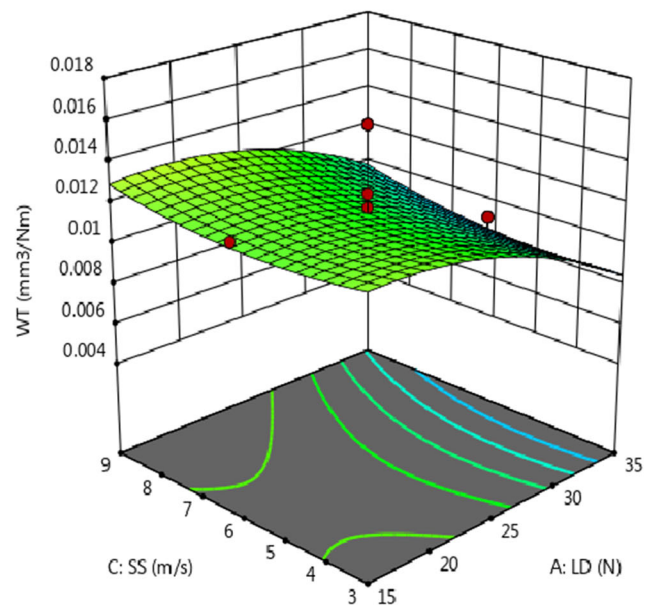
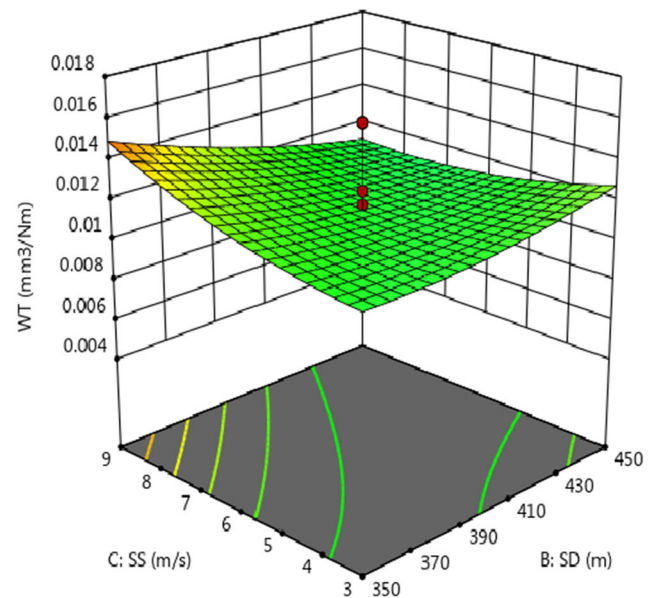


Fig. 7 SS/SD interaction plot



comparing it to experimental data [36–40]. Model adequacy is examined using  $R^2$ , adjusted  $R^2$ , and anticipated  $R^2$ .  $R^2$  denotes the percentage of overall variation in the model-predicted response. The better correlation coefficients testify to the models' suitability and the accuracy of the derived constants. In regression analysis, the projected  $R^2$  is used to show how accurately the model predicts outcomes for product observations. When comparing models, predicted  $R^2$  can

be more helpful than adjusted  $R^2$  because it is determined using observations that are not considered during model estimation [32]. The  $R^2$  values is 0.9678 response of wear rate which ensures a satisfactory fit of the model to the experimental data.

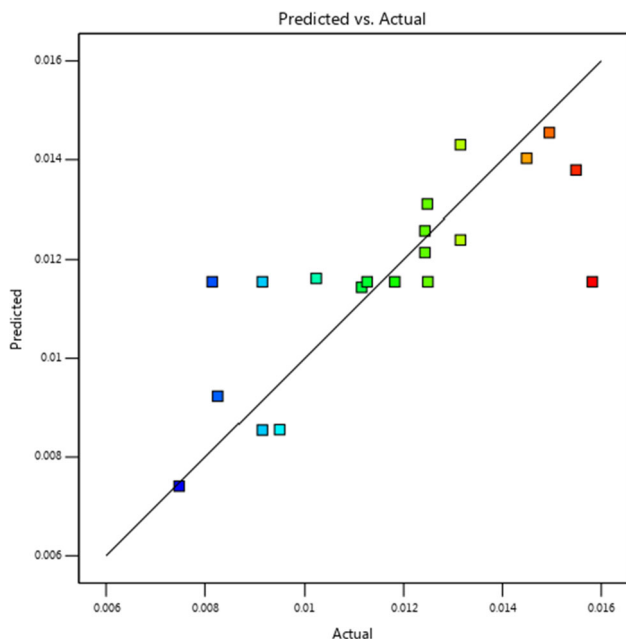


Fig. 8 Actual versus predicted plot

### 7 SEM analysis on worn out surfaces

The surface conditions of workpiece before & after wear test are displayed in Figs. 10 and 11 respectively, the reinforcements are dispersed in Al alloy in all over region and clearly visible in Fig. 10. Figure 11 shows that SEM picture of Experiment no: 15 under the load – 25N, sliding distance – 400 mm and sliding speed – 6 m/s. the formation of debris, groves and cavity are produced due to ploughing action on the surface. The worn surfaces of the Al based composite at 6 m/s reveal finer grooves at right side of the surface and

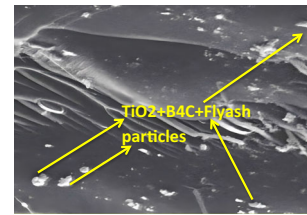


Fig. 10 SEM image of sample of experiment no: 15

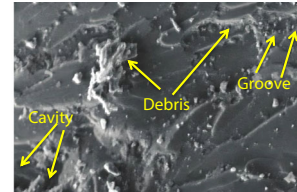


Fig. 11 SEM image of sample no: 15 after wear test

small plastic distortion at the groove edge due to better wear resistance. Due to application of load 25 N, the debris and cavities are produced more especially in center and left corner regions.

### 8 Conclusion

In the current work, Al7178/TiO<sub>2</sub>/B4C/FA hybrid composite are produced by stir casting method. Pin on disc equipment is selected to execute wear test as per the CCD design. Wear parameters have been analyzed via design expert software. The influenced parameters load, sliding speed, sliding distance and reinforcement on the output response of wear rate

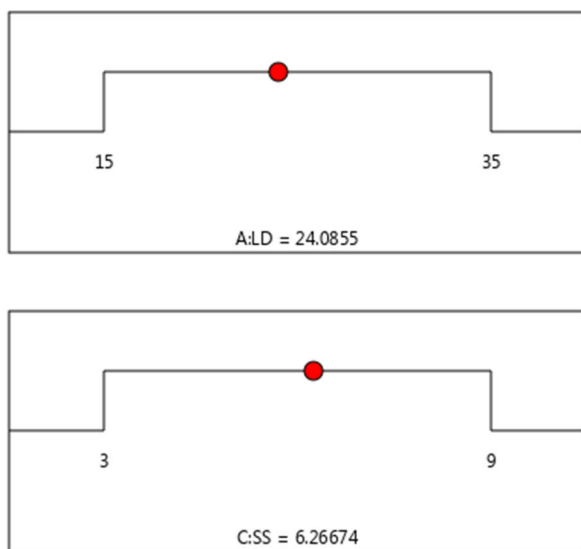
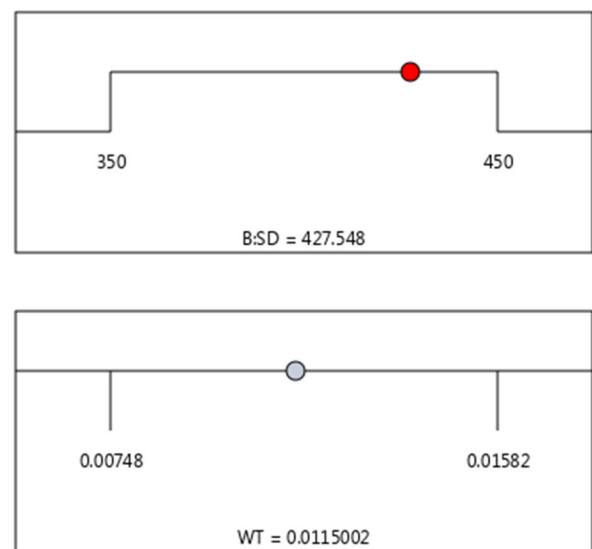


Fig. 9 Graph for predicting wear rate with variation of wear factors



were investigated. ANOVA supports to determine the significant process parameters. According to observed results, the following conclusions can be drawn as mentioned-below.

- Load (LD) is significantly affect Wear rate (WT) and ANOVA exposes that the interaction between LD \*SD, LD\*SS and SS\*SD on the effect of the wear rate.
- An increase in both load and sliding distance increases the WT, whereas decreasing reinforcement and sliding speed lead to a decrease in WT
- The contour plot can be used to evaluate and examine process factors influences the wear rate. shows that Maximum wear rate is recorded as  $0.01582 \text{ mm}^3/\text{Nm}$  For load of 25 N, slide distance of 400 m and slide speed of 6 m/s.
- The minimum Wear rate is attained as  $0.00748 \text{ mm}^3/\text{Nm}$  at parameters combinations of 35 N, 450 m and 9 m/s. Analysis of variance (ANOVA) showed that load, and the interaction between Load and sliding distance have the most significant parameters on wear rate trailed by sliding speed.

## References

1. Christy, J.V., Arunachalam, R., Mourad, A.H.I., Krishnan, P.K., Piya, S., Al-Maharbi, M.: Processing, properties, and microstructure of recycled aluminum alloy composites produced through an optimized stir and squeeze casting processes. *J. Manuf. Process.* **59**, 287 (2020)
2. Karthik, A., Karunanithi, R., Srinivasan, S.A., Prashanth, M.: The optimization of squeeze casting process parameter for AA2219 alloy by using the Taguchi method. *Mater. Today Proc.* **27**, 2556–2561 (2020)
3. Pydi, H.P., Pradeep, A., Vijayakumar, S., Srinivasan, R.: Examination of various weld process parameters in MIG welding of carbon steel on weld quality using radiography and magnetic particle testing. *Mater. Today Proc.* **62**, 1–4 (2022)
4. Paramasivam, P., Vijayakumar, S.: Mechanical characterization of aluminium alloy 6063 using destructive and non-destructive testing. *Mater. Today Proc.* (2021). <https://doi.org/10.1016/j.matpr.2021.04.312>
5. Gugulothu, B., Nagarajan, N., Pradeep, A., Saravanan, G., Vijayakumar, S., Rao, J.: Analysis of mechanical properties for Al-MMC fabricated through an optimized stir casting process. *J. Nanomater.* **2022**, 1–7 (2022). <https://doi.org/10.1155/2022/2081189>
6. Kumar, S.D., Ravichandran, M.: Synthesis, characterization and wire electric erosion behaviour of AA7178–10 wt% ZrB<sub>2</sub> composite. *Siliconindia* **10**, 2653–2662 (2018). <https://doi.org/10.1007/s12633-018-9802-7>
7. Rajan, H.B.M., Ramabalan, S., Dinaharan, I., Vijay, S.J.: Synthesis and characterization of in situ formed titanium diboride particulate reinforced AA7075 aluminum alloy cast composites. *Mater. Des.* **44**, 438–445 (2013). <https://doi.org/10.1016/j.matdes.2012.08.008>
8. Baskaran, S., Anandakrishnan, V., Duraiselvam, M.: Investigations on dry sliding wear behavior of in situ casted Journal of Nanomaterials 7AA7075-TiC metal matrix composites by using Taguchi technique. *Mater. Des.* **60**, 184–192 (2014)
9. K ok, M.: Prediction and optimisation of abrasive wear model for particulate reinforced MMCs using statistical analysis. *Mater. Res. Innov.* **15**(5), 366–372 (2011)
10. Vithal, D.N., Krishna, B.B., Krishna, G.M.: Microstructure, mechanical properties and fracture mechanisms of ZrB<sub>2</sub> ceramic reinforced A7075 composites fabricated by stir casting. In: *Materials Today Communications*, vol. 25, p. 101289. Elsevier (2020). <https://doi.org/10.1016/j.mtcomm.2020.101289>
11. Kumar, S.D., Ravichandran, M., Jeevika, A., Stalin, B., Kailasanathan, C., Karthick, A.: Effect of ZrB<sub>2</sub> on microstructural, mechanical and corrosion behaviour of aluminium (AA7178) alloy matrix composite prepared by the stir casting route. In: *Ceramics International*, vol. 47, Issue 9, pp. 12951–12962. Elsevier (2021). <https://doi.org/10.1016/j.ceramint.2021.01.158>
12. Kumar, A., Patnaik, A., Bhat, I.K.: Investigation of nickel metal powder on tribological and mechanical properties of Al-7075 alloy composites for gear materials. *Powder Metall.* **60**(5), 371–383 (2017)
13. Kumar, G.B.V., Rao, C.S.P., Selvaraj, N.: Mechanical and dry sliding wear behavior of Al7075 alloy-reinforced with SiC particles. *J. Compos. Mater.* **46**(10), 1201–1209 (2012)
14. Ambigai, R., Prabhhu, S.: Optimization of friction and wear behaviour of Al-Si<sub>3</sub>N<sub>4</sub> nano composite and Al-Gr-Si<sub>3</sub>N<sub>4</sub> hybrid composite under dry sliding conditions. *Trans. Nonferrous Met. Soc. China* **27**(5), 986–997 (2017)
15. Bharath, V., Nagara, M., Auradi, V., Kori, S.A.: Preparation of 6061Al-Al<sub>2</sub>O<sub>3</sub> MMC's by stir casting and evaluation of mechanical and wear properties. *Proc. Mater. Sci.* **6**, 1658–1667 (2014). <https://doi.org/10.1016/j.mspro.2014.07.151>
16. Radha Krishnan, B., Theerkka Tharisanan, R., Arumuga Prabu, V., Immanuel, P., Ramakrishnan, A.: Experimental investigation of mechanical properties of Al7075-Al<sub>2</sub>O<sub>3</sub>-B<sub>4</sub>C composite via stir route. *Mater. Today Proc.* **64**, 1721–1724 (2022). <https://doi.org/10.1016/j.matpr.2022.05.498>
17. Gugulothu, B., Sankar, S.L., Vijayakumar, S., Prasad, A.S.V., Thangaraj, M., Venkatachalapathy, M., Rao, T.V.J.: Analysis of wear behaviour of AA5052 alloy composites by addition alumina with zirconium dioxide using the Taguchi-grey relational method. *Adv. Mater. Sci. Eng.* **2022**, 1–7 (2022). <https://doi.org/10.1155/2022/4545531>
18. Pal, D., Vijayakumar, S., Rao, T.V.J., Babu, R.S.R.: An examination of the tensile strength, hardness and SEM analysis of Al 5456 alloy by addition of different percentage of SiC/flyash. *Mater. Today Proc.* (2022). <https://doi.org/10.1016/j.matpr.2022.02.288>
19. Boopathy, G., Vanitha, V., Karthiga, K., Gugulothu, B., Pradeep, A., Pydi, H.P., Vijayakumar, S.: Optimization of tensile and impact strength for injection moulded nylon 66/SiC/B<sub>4</sub>c composites. *J. Nanomater.* **2022**, 1–9 (2022). <https://doi.org/10.1155/2022/4920774>
20. Gugulothu, B., Anusha, P., Swapna Sri, M.N., Vijayakumar, S., Periyasamy, R., Seetharaman, S.: Optimization of stir-squeeze casting parameters to analyze the mechanical properties of Al7475/B<sub>4</sub>C/Al<sub>2</sub>O<sub>3</sub>/TiB<sub>2</sub> hybrid composites by the Taguchi method. *Adv. Mater. Sci. Eng.* **2022**, 1–9 (2022). <https://doi.org/10.1155/2022/3180442>
21. Vijayakumar, S., SatheshKumar, P.S., Sampathkumar, P., Manickam, S., Ramaiah, G.B., Pydi, H.P.: The effect of stir-squeeze casting process parameters on mechanical property and density of aluminum matrix composite. In: Khan, M.A. (ed.) *Advances in Materials Science and Engineering*, vol. 2022, pp. 1–10. Hindawi Limited (2022). <https://doi.org/10.1155/2022/3741718>
22. Dhawan, A., et al.: Evaluation of mechanical properties of concrete manufactured with fly ash, bagasse ash and banana fibre. *Mater. Today Proc.* **44**, 17–22 (2021)



23. Gupta, N., et al.: Mechanical and durability properties of geopolymer concrete composite at varying superplasticizer dosage. *Mater. Today Proc.* **44**, 12–16 (2021)
24. Kumar, N., Bharti, A., Saxena, K.K.: A re-investigation: effect of powder metallurgy parameters on the physical and mechanical properties of aluminium matrix composites. *Mater. Today Proc.* **44**, 2188–2193 (2021)
25. Rajput, S.K., et al.: Microstructural evolution and mechanical properties of 316L stainless steel using multi-axial forging. *Adv. Mater. Process. Technol.* **6**(3), 509–518 (2020)
26. Samyal, R., et al.: Predicting the effect of fiber orientations and boundary conditions on the optimal placement of PZT sensor on the composite structures. *Mater. Res. Express* **8**(7), 75302 (2021)
27. Saxena, K.K., et al.: A novel approach to understand the deformation behavior in two phase region using processing map. *J. Alloys Compd.* **706**, 511–519 (2017)
28. Upadhyay, S., Saxena, K.K.: ‘Effect of Cu and Mo addition on mechanical properties and microstructure of grey cast iron: an overview. *Mater. Today Proc.* **26**, 2462–2470 (2020)
29. Rajmohan, T., Palanikumar, K., Ranganathan, S.: Evaluation of mechanical and wear properties of hybrid aluminium matrix composites. *Trans. Nonferrous Met. Soc. China* **23**(9), 2509–2517 (2013)
30. Gopalakrishnan, S., Murugan, N.: Production and wear characterisation of AA 6061 matrix titanium carbide particulate reinforced composite by enhanced stir casting method. *Compos. Part B Eng.* **43**(2), 302–308 (2012). <https://doi.org/10.1016/j.compositesb.2011.08.049>
31. Hong, X., Xin, Z., Yanpeng, L., Yang, S., Jiping, R., Changshun, W.: Mechanical property and corrosion behavior of SiCp/2A50 composites prepared by liquid forging. *Rare Met. Mater. Eng.* **44**(6), 1307–1313 (2015). [https://doi.org/10.1016/s1875-5372\(15\)30080-1](https://doi.org/10.1016/s1875-5372(15)30080-1)
32. Yaghoobi, H., Fereidoon, A.: Thermal analysis, statistical predicting, and optimization of the flexural properties of natural fiber biocomposites using Box–Behnken experimental design. *J. Natl. Fibers* **16**(7), 987–1005 (2019). <https://doi.org/10.1080/15440478.2018.1447416>
33. Raj, I.L.P., Valanarasu, S., Hariprasad, K., Ponraj, J.S., Chidhambaram, N., Ganesh, V., Khairy, Y.: Enhancement of optoelectronic parameters of Nd-doped ZnO nanowires for photodetector applications. *Opt. Mater.* **109**, 110396 (2020). <https://doi.org/10.1016/j.optmat.2020.110396>
34. Dhanalaxmi, B., Naidu, G.A., Anuradha, K.: Adaptive PSO based association rule mining technique for software defect classification using ANN. *Proc. Comput. Sci.* **46**, 432–442 (2015). <https://doi.org/10.1016/j.procs.2015.02.041>
35. Krishnamoorthy, N., Prasad, L.N., Kumar, C.P., Subedi, B., Abraha, H.B., Sathishkumar, V.E.: Rice leaf diseases prediction using deep neural networks with transfer learning. *Environ. Res.* **198**, 111275 (2021). <https://doi.org/10.1016/j.envres.2021.111275>
36. Atchudan, R., Edison, T.N.J.I., Mani, S., Perumal, S., Vinodh, R., Thirunavukkarasu, S., Lee, Y.R.: Facile synthesis of a novel nitrogen-doped carbon dot adorned zinc oxide composite for photodegradation of methylene blue. *Dalton Trans.* **49**(48), 17725–17736 (2020). <https://doi.org/10.1039/D0DT02756A>
37. Sai Shravan Kumar, P., Viswanath Allamraju, K.: A review of natural fiber composites [Jute, Sisal, Kenaf]. *Mater. Today Proc.* **18**(7), 2556–2562 (2019). <https://doi.org/10.1016/j.matpr.2019.07.113>
38. Bhavana, G., et al.: Design and implementation of vehicle navigation system in urban environments using internet of things (Iot). In: 2017 IOP Conference Series Material Science and Engineering, vol. 225, p. 012262. <https://doi.org/10.1088/1757-899X/225/1/012262>
39. Budarapu, P.R., Yb, S.S., Javvaji, B., et al.: Vibration analysis of multi-walled carbon nanotubes embedded in elastic medium. *Front. Struct. Civ. Eng.* **8**, 151–159 (2014). <https://doi.org/10.1007/s11709-014-0247-9>
40. Bhukya, M.N., Kota, V.R., Depuru, S.R.: A simple, efficient, and novel standalone photovoltaic inverter configuration with reduced harmonic distortion. *IEEE Access* **7**, 43831–43845 (2019). <https://doi.org/10.1109/ACCESS.2019.2902979>

**Publisher’s Note** Springer Nature remains neutral with regard to jurisdictional claims in published maps and institutional affiliations.

Springer Nature or its licensor (e.g. a society or other partner) holds exclusive rights to this article under a publishing agreement with the author(s) or other rightsholder(s); author self-archiving of the accepted manuscript version of this article is solely governed by the terms of such publishing agreement and applicable law.